AIMETA 2017
XXIII Conference
The Italian Association of Theoretical and Applied Mechanics
Luigi Ascione, Valentino Berardi, Luciano Feo, Fernando Fraternali and Antonio Michele Tralli (eds.)
Salerno, Italy, 4-7 September 2017

AN ELASTIC-INTERFACE MODEL FOR BUCKLING-DRIVEN DELAMINATION GROWTH IN FOUR-POINT BENDING TESTS

Stefano Bennati[1], **Nicola Dardano**[2], **Paolo S. Valvo**[1]

[1] University of Pisa, Department of Civil and Industrial Engineering
Largo Lucio Lazzarino, 56122 Pisa, Italy
e-mail: {s.bennati, p.valvo}@ing.unipi.it

[2] IMT School for Advanced Studies Lucca
Piazza San Francesco 19, 55100 Lucca, Italy
e-mail: nicola.dardano@imtlucca.it

Keywords: Composite laminate, delamination buckling, four-point bending test, interface model.

Abstract. *The paper presents a mechanical model of a four-point bending test on a delaminated specimen, considered as an assemblage of laminated beams partly connected by an elastic interface. A differential problem with suitable boundary conditions is formulated to describe the model. Then, an analytical solution is determined for both the pre- and post-critical stages. A mixed-mode fracture criterion is applied to predict the onset of delamination growth. The model is illustrated through comparison with some experimental results taken from the literature.*

1 INTRODUCTION

Delamination, or interlaminar fracture, is a major failure mode for composite laminates. Interlaminar cracks may have many causes – such as manufacturing defects or low-energy impacts – and propagate under static or dynamic loads producing high interlaminar stresses. In particular, local buckling in the region of an existing delamination may promote further crack extension [1].

In this paper, we analyse the delamination growth promoted by local buckling in a composite laminate with a central, through-the-width delamination, subjected to four-point bending test [2]. By extending an approach already adopted to analyse delamination buckling in a different problem [3, 4], we model the specimen as an assemblage of sublaminates, some of which are connected by an elastic interface. Thanks to symmetry, the analysis is limited to the left-hand half of the specimen, which is subdivided into three zones: a first zone, between the support and the load application point, where the specimen is schematised as a single laminate; a second zone, between the load application point and the delamination front, where the specimen consists of two sub-laminates connected by the elastic interface; a third zone, between the delamination front and the symmetry axis, where the two previous sub-laminates are not connected by the interface. All sub-laminates are considered as extensible and flexible beams undergoing small elastic deformations, except for the compressed sub-laminate in the third zone, which may undergo large displacements.

The mechanical problem is described by a set of differential equations with suitable boundary conditions, which are solved analytically in the pre- and post-critical stages. The buckling load is determined through the numerical solution of a suitable transcendental equation. In the post-critical stage, the energy release rate and mode mixity are evaluated to predict the load corresponding to the onset of delamination growth. The theoretical predictions of the model are in good agreement with some experimental results of the literature [5–7].

2 FORMULATION OF THE PROBLEM

2.1 Mechanical model

Let us consider a laminate of length $2L$, whose cross section has thickness H and width B. A delamination crack of length $2a$ is present at the mid-span cross section at distances H_1 and H_2 from the top and bottom surfaces of the laminate, respectively. The laminate is subjected to four-point bending test with two loads of intensity P, both placed at distances l_1 from the outer supports and l_2 from the delamination crack tips (Figure 1).

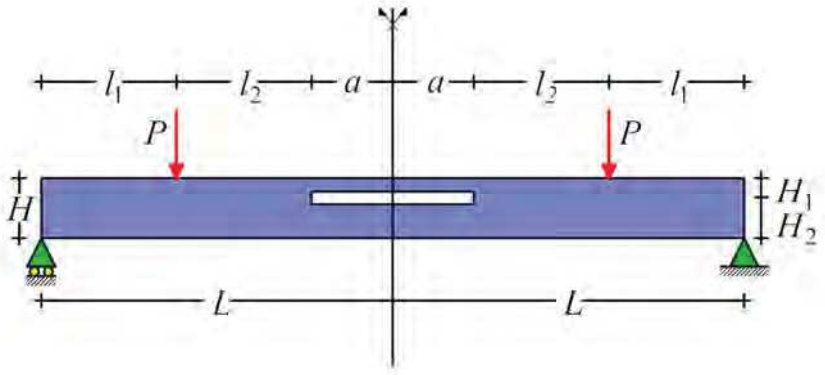

Figure 1: test specimen.

The mechanical model considers the specimen as an assemblage of sub-laminates. Due to the symmetry of the problem, it is possible to limit the study to the left-hand half specimen by introducing appropriate constraints at the symmetry axis (Figure 2). In particular, the model can be divided into three zones with different behaviour: a first zone of length l_1, between the support and the load application point, in which the laminate is schematised as a single sub-laminate (1); a second zone of length l_2, between the load application point and the delamination crack tip, in which the laminate is schematised as two sub-laminates (2) and (3) connected by an elastic interface; lastly, a third zone of length a, where the laminate consists of two unconnected sub-laminates (4) and (5). Three local abscissas, s_1, s_2, and s_3, are used in each zone.

All sub-laminates are considered as extensible and flexible elastic beams. Sub-laminate (4) is modelled according to Euler's model for beam-columns in compression. The different modelling assumption for sub-laminate (4) is consistent with experimental evidence, showing that this portion undergoes compression and eventually buckles under high testing loads. Let A_i and J_i (i = 1, 2, …, 5) respectively denote the area and moment of inertia of sub-laminates (with $A_4 = A_2$, $J_4 = J_2$, $A_5 = A_3$, and $J_5 = J_3$). The longitudinal Young's modulus $E = E_1$ is considered constant throughout the specimen. Let v_i, w_i and φ_i, respectively denote the transverse and axial displacements, and rotations (positive if clockwise) of a generic cross section.

The elastic interface is considered as a continuous distribution of linearly elastic springs acting in the normal and tangential directions with respect to the interface plane. Let k_y and k_z respectively denote the elastic interface constants in the normal and tangential directions.

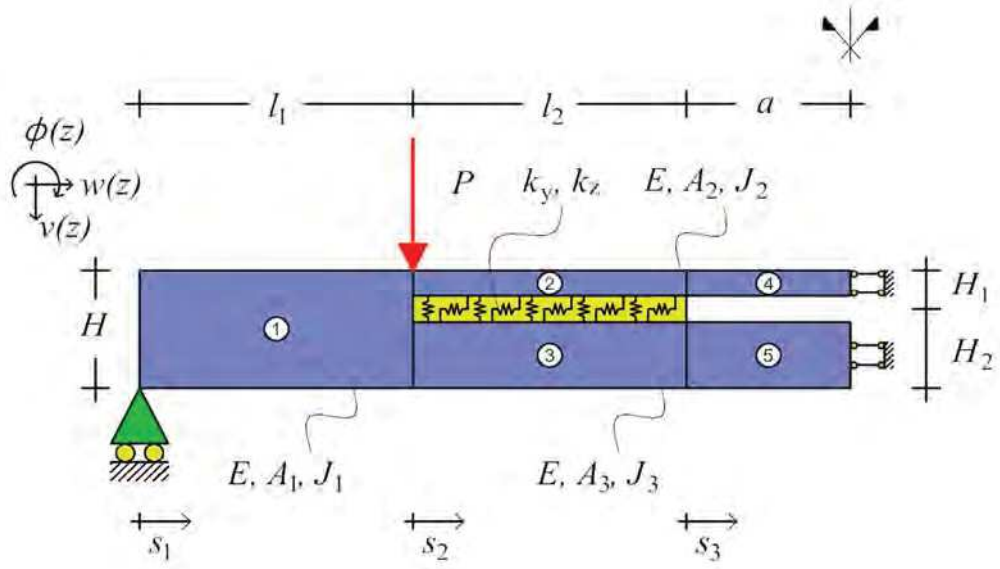

Figure 2: mechanical model.

2.2 Differential problem

As described in detail in [8], by imposing static equilibrium and accounting for the constitutive laws, the following differential problem is obtained that describes the elastic response of the specimen in the pre- and post-critical stages:

$$\begin{cases} EJ_1 v_1^{\mathrm{IV}}(s_1) = 0 \\ EA_1 w_1^{\mathrm{II}}(s_1) = 0 \\ EJ_2 v_2^{\mathrm{IV}}(s_2) - Bk_y\big(v_3(s_2) - v_2(s_2)\big) - \frac{1}{2}H_1 EA_2 w_2^{\mathrm{III}}(s_2) = 0 \\ EA_2 w_2^{\mathrm{II}}(s_2) = Bk_z\left(w_3(s_2) - w_2(s_2) + \frac{1}{2}H_2 v_3^{I}(s_2) + \frac{1}{2}H_1 v_2^{I}(s_2)\right) \\ EJ_3 v_3^{\mathrm{IV}}(s_2) + Bk_y\big(v_3(s_2) - v_2(s_2)\big) + \frac{1}{2}H_1 EA_3 w_3^{\mathrm{III}}(s_2) = 0 \\ EA_3 w_3^{\mathrm{II}}(s_2) = -Bk_z\left(w_3(s_2) - w_2(s_2) + \frac{1}{2}H_2 v_3^{I}(s_2) + \frac{1}{2}H_1 v_2^{I}(s_2)\right) \\ EJ_2 v_4^{\mathrm{IV}}(s_3) = \begin{cases} 0 & \text{pre-critical stage} \\ -P_4 v_4^{\mathrm{II}}(s_3) & \text{post-critical stage} \end{cases} \\ EA_2 w_4^{\mathrm{II}}(s_3) = 0 \\ EJ_3 v_5^{\mathrm{IV}}(s_3) = 0 \\ EA_3 w_5^{\mathrm{II}}(s_3) = 0 \end{cases} \tag{1}$$

where $P_4 = -N_4$ is the compressive axial force in sub-laminate (4).

2.3 Boundary conditions

The solution of the differential problem (1) will be different in the pre- and post-critical stages. In both cases, the solution includes thirty unknown integration constants. To determine these, the differential problem needs to be completed by thirty boundary conditions, which guarantee balance and kinematical compatibility at the end cross sections of sub-laminates:

$$\begin{gathered} v_1(0) = 0; \qquad M_1(0) = 0; \qquad N_1(0) = 0; \\ v_1(l_1) = v_2(0); \quad v_1(l_1) = v_3(0); \qquad \phi_1(l_1) = \phi_2(0); \qquad \phi_1(l_1) = \phi_3(0); \\ M_1(l_1) = M_2(0) + M_3(0) - \frac{1}{2}H_2 N_2(0) + \frac{1}{2}H_1 N_2(0); \qquad T_1(l_1) - P = T_2(0) + T_3(0); \\ w_1(l_1) - \frac{1}{2}H_2\phi_1(l_1) = w_2(0); \quad w_1(l_1) + \frac{1}{2}H_1\phi_1(l_1) = w_3(0); \quad N_1(l_1) = N_2(0) + N_3(0); \\ v_2(l_2) = v_4(0); \qquad \phi_2(l_2) = \phi_4(0); \qquad M_2(l_2) = M_4(0); \qquad T_2(l_2) = T_4(0); \\ w_2(l_2) = w_4(0); \qquad N_2(l_2) = N_4(0); \qquad v_3(l_2) = v_5(0); \qquad \phi_3(l_2) = \phi_5(0); \\ M_3(l_2) = M_5(0); \qquad T_3(l_2) = T_5(0); \qquad w_3(l_2) = w_5(0); \qquad N_3(l_2) = N_5(0); \\ \phi_4(a) = 0; \quad T_4(a) = 0; \quad w_4(a) = 0; \\ \phi_5(a) = 0; \quad T_5(a) = 0; \quad w_5(a) = 0. \end{gathered} \tag{2}$$

Formally, the boundary conditions are the same in pre- and post-critical stages. However, when substituting the corresponding solutions of Eqs. (1) into (2), two different sets of equations are obtained in the two stages. In the pre-critical stage, the system of boundary conditions does not involve particular difficulties because it furnishes a single solution for the integration constants, which are all linear in the load intensity, P. In the post-critical stage, instead, the solution of the boundary condition system is complicated by the fact that the solution of the differential problem depends non-linearly on the axial force P_4. To overcome this difficulty, the adopted solution strategy is to represent the solution as a function of the parameter P_4, by introducing the applied bending moment, $M = P\, l_1$, as an auxiliary unknown.

3 SOLUTION OF THE PROBLEM

As described in detail in [8], by suitable manipulation, the system of differential equations is uncoupled and solved, yielding the following general solution:

$$v_1(s_1) = C_1 {s_1}^3 + C_2 {s_1}^2 + C_3 s_1 + C_4 \tag{3}$$

$$w_1(s_1) = C_5 s_1 + C_6 \tag{4}$$

$$v_2(s_2) = \frac{D_1 k_y}{2}\Big((\alpha^2+\beta^2)\big(C_{11}\zeta_2 H_1 \sin(\gamma s_2) - C_{12}\zeta_2 H_1 \cos(\gamma s_2) + 2\gamma H_2 (D_2 {s_2}^3 + D_3 {s_2}^2 + D_4 s_2 + D_5) k_y\big) + \gamma H_1 \sinh(\alpha s_2)\big(\sin(\beta s_2)(\alpha C_8 \omega_2 - \beta C_9 \chi_2) + \cos(\beta s_2)(\alpha C_7 \omega_2 + \beta C_{10}\chi_2)\big) + \gamma H_1 \cosh(\alpha s_2)\big(\sin(\beta s_2)(\alpha C_{10}\omega_2 - \beta C_7 \chi_2) + \cos(\beta s_2)(\alpha C_9 \omega_2 + \beta C_8 \chi_2)\big)\Big) \tag{5}$$

$$w_2(s_2) = cosh(\alpha s_2)(C_7\, cos(\beta s_2) + C_8\, sin(\beta s_2)) + sinh(\alpha s_2)(C_9\, cos(\beta s_2) + C_{10}\, sin(\beta s_2)) + C_{12}\, sin(\gamma s_2) + C_{11}\, cos(\gamma s_2) + C_{15} {s_2}^2 + C_{14} s_2 + C_{13} \tag{6}$$

$$v_3(s_2) = D_1\Big((\alpha^2+\beta^2)\big(-6C_{11}\zeta_3 H_1 \sin(\gamma s_2) + 6C_{12}\zeta_3 H_1 \cos(\gamma s_2) + \gamma H_2 (D_2 {s_2}^3 + D_3 {s_2}^2 + D_4 s_2 + D_5)\big) + 6\gamma H_1 \sinh(\alpha s_2)\big(\sin(\beta s_2)(\alpha C_8 \omega_3 - \beta C_9 \chi_3) + \cos(\beta s_2)(\alpha C_7 \omega_3 + \beta C_{10}\chi_3)\big) + 6\gamma H_1 \cosh(\alpha s_2)\big(\sin(\beta s_2)(\alpha C_{10}\omega_3 - \beta C_7 \chi_3) + \cos(\beta s_2)(\alpha C_9 \omega_3 + \beta C_8 \chi_3)\big)\Big) \tag{7}$$

$$w_3(s_2) = -\frac{H_1}{H_2}(\cosh(\alpha s_2)(C_7 \cos(\beta s_2) + C_8 \sin(\beta s_2)) + \sinh(\alpha s_2)(C_9 \cos(\beta s_2) + C_{10} \sin(\beta s_2)) + C_{12} \sin(\gamma s_2) + C_{11} \cos(\gamma s_2) + C_{15} {s_2}^2) + C_{17} s_2 + C_{16} \tag{8}$$

$$v_4(s_3) = \begin{cases} C_{21} + C_{22} s_3 + C_{23} {s_3}^2 + C_{24} {s_3}^3 & \text{pre-critical stage} \\ C_{21}\, cos(\lambda_c s_3) + C_{22}\, sin(\lambda_c s_3) + C_{23} + C_{24} s_3 & \text{post-critical stage} \end{cases} \tag{9}$$

$$w_4(s_3) = C_{19} + C_{20} s_3 \tag{10}$$

$$v_5(s_3) = C_{27} + C_{28} s_3 + C_{29} {s_3}^2 + C_{30} {s_3}^3 \tag{11}$$

$$w_5(s_3) = C_{25} + C_{26} s_3 \tag{12}$$

where C_1, C_2, …, C_{30} are the main integration constants; in addition, α, β and γ are three real constants, which describe the roots of the characteristic polynomial of the differential equation for the sublaminates (2) and (3) [8]. The roots of the characteristic polynomial have the following form (where i denotes the imaginary unit):

$$\lambda_1 = -\gamma\mathrm{i};\ \lambda_2 = +\gamma\mathrm{i};\ \lambda_3 = -\alpha + \beta\mathrm{i};\ \lambda_4 = +\alpha - \beta\mathrm{i}; \tag{13}$$

$$\lambda_5 = -\alpha - \beta;\ \lambda_6 = \alpha + \beta\mathrm{i};\ \lambda_7 = \lambda_8 = \lambda_9 = 0; \tag{14}$$

D_1, D_2,…, D_5, χ_2, ω_2, ζ_2, χ_3, ω_3, ξ_3 are constants, whose expressions are given in the Appendix.

4 NUMERICAL EXAMPLE

To better understand the predicted behaviour of the specimen, we consider a numerical example and compare our theoretical predictions to experimental results taken from the literature. It should be pointed out that our model furnishes acceptable predictions only if there is no contact and interpenetration between sub-laminates (4) and (5). For this reason, appropriate constraints are introduced in the following.

4.1 Geometric and mechanical characteristics

The geometric and mechanical properties of the specimen correspond to what reported by Kinawy et al. [7]. These are summarized in Tables 1 and 2.

H (mm)	a (mm)	l_1 (mm)	l_2 (mm)	H_1 (mm)	H_2 (mm)	B (mm)
4.25	20	15	$60 - a$	$H/8$	$H - H_1$	10.27

Table 1: geometric characteristics of the specimen.

E_1 (N/mm^2)	E_3 (N/mm^2)	G_{31} (N/mm^2)	G_{Ic} (J/m^2)	G_{IIc} (J/m^2)
139000	9000	4980	550	1400

Table 2: mechanical characteristics of the specimen.

Table 3 shows the values of the stiffness constants of the elastic interface, k_y and k_z. These have been calibrated to match the experimental results of Kinaway et al. [7] in the pre- and post-critical stages.

k_z (N/mm^3)	k_y (N/mm^3)
475.11	732.35

Table 3: stiffness constants of the elastic interface.

4.2 Behaviour of the specimen in post-critical stage

After solving the system of boundary conditions Eqs. (2), with the above-mentioned strategy, we found the trend of the applied bending moment, $M = P\, l_1$, vs. the compressive axial force of sub-laminate (4), P_4 (Figure 3). Also, we determined the trend of the applied bending moment vs. the relative displacement between the sub-laminates (4) and (5), $\Delta v(a)$, at the mid-span cross section (Figure 4).

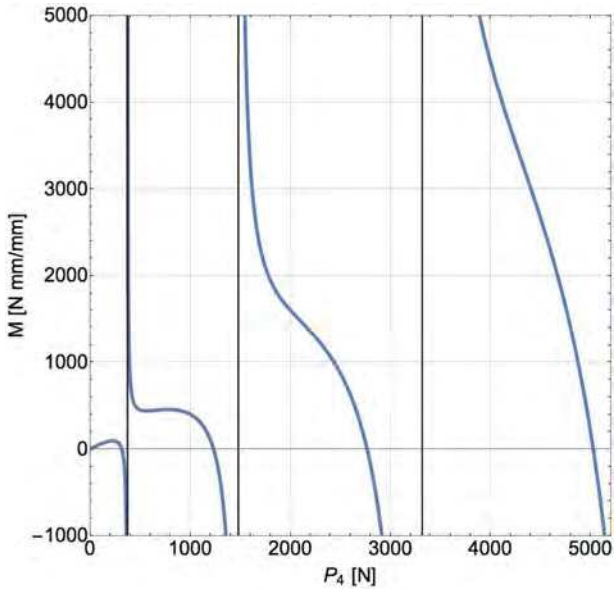

Figure 3: applied bending moment vs. axial force of sub-laminate (4)

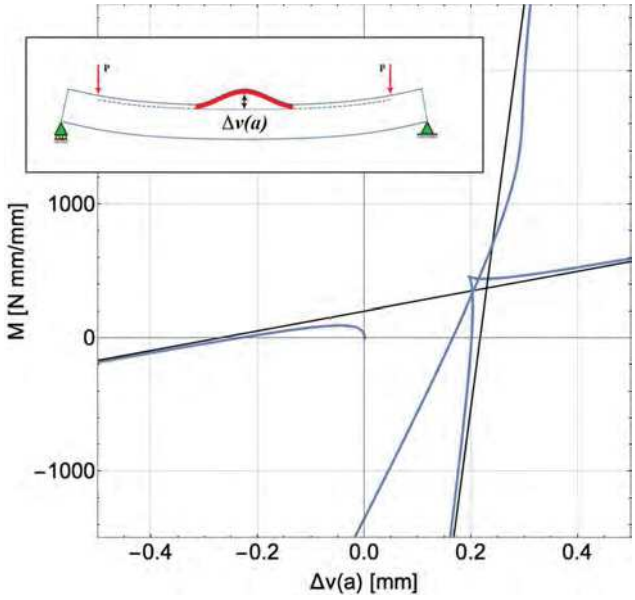

Figure 4: applied bending moment vs. relative displacement between the sub-laminates (4) and (5).

The curves shown in Figures 3 and 4 represent all theoretical solution points. However, at a closer examination, it appears that some portions of the solution curves must be excluded because they represent physically unfeasible states. For example, all those points in which the applied bending moment is negative are to be excluded as they would require negative, i.e. upwards directed, loads. Instead, in the four-point bending test, the testing machine always applies downward loads. Moreover, Figure 4 shows some equilibrium paths where the sub-laminates (4) and (5) are in contact, where $\Delta v(a) = 0$, or interpenetrate, where $\Delta v(a) < 0$. Also, these solutions are physically unfeasible. A further limitation is given by the compressive strength of sub-laminate (4), which must not be overcome. Thus, by excluding also these physically unacceptable solutions, we finally arrive at the desired physically feasible solution path.

Figures 5 and 6 respectively correspond to Figures 3 and 4 after the physically unfeasible solutions have been excluded. The unfeasible paths are represented by dashed blue lines and the feasible ones by a continuous red line. The pre-critical path in Figure 6 has been traced simply by assuming that sub-laminates (4) and (5) stay in contact until instability occurs, as experimentally observed by many researchers [5-7, 9]. Also in line with experimental evidence, we expect that instability will not occur through equilibrium bifurcation, but snapping. Finally, in Figure 6, we have plotted with grey dots the experimental results by Kinawy et al. [5-7] for comparison with our model.

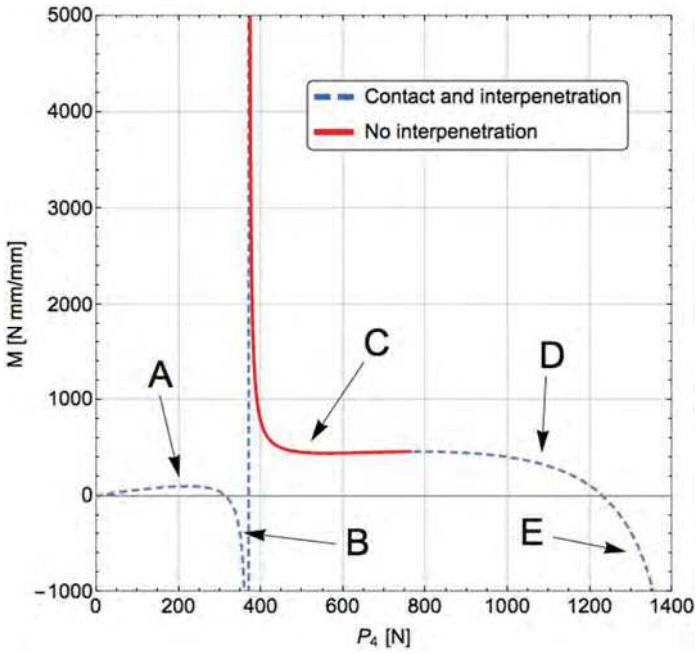

Figure 5: applied bending moment vs normal stress P_4 of sub-laminate (4)

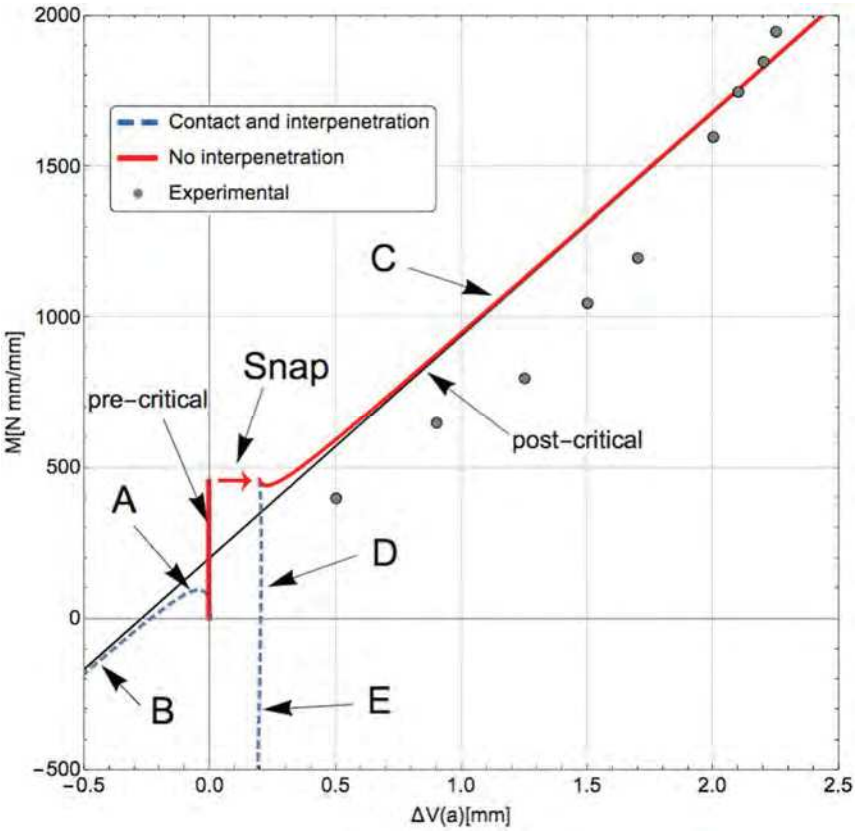

Figure 6: predicted response and experimental data.

Further insight into the predicted behaviour can be obtained by inspection of Figure 7, which illustrates the deformed configurations corresponding to solution paths A, B, C, D, and E. Only path C is feasible, as it does not feature upward loads and interpenetration.

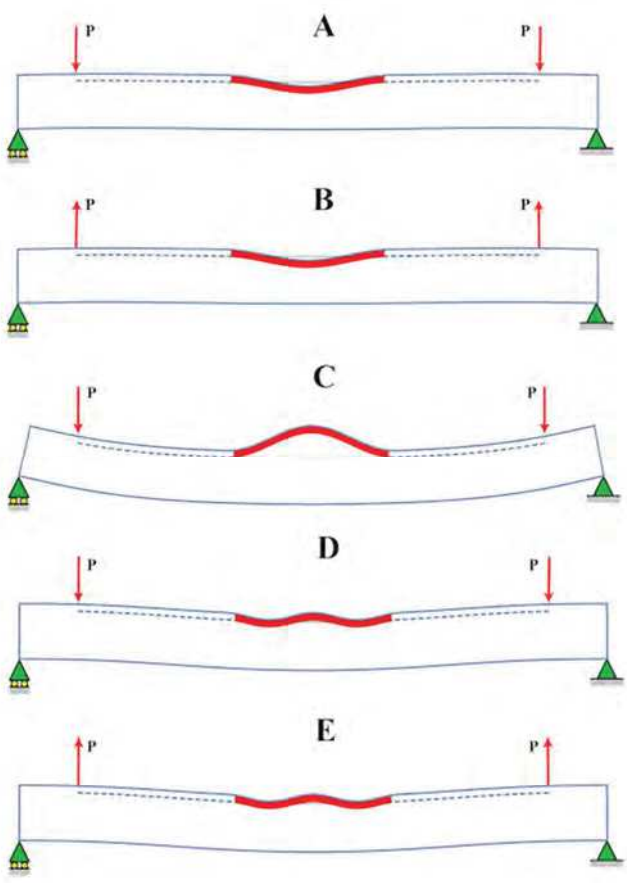

Figure 7: deformed configurations of the specimen for each solution path.

4.3 Prediction of delamination growth

In the post-critical stage, we expect a progressive increase in the interfacial stresses, eventually leading to further growth of the delamination crack. Since both normal and tangential stresses are present at the crack tips, fracture will occur under I/II mixed-mode conditions. To predict the onset of delamination growth, we first evaluate the energy release rate and mode mixity. Then, we compare the available energy release rate with the critical value according to the criterion of Hutchinson and Suo [10].

The normal and tangential stresses at the crack tip ($s_2 = l_2$) respectively are

$$\sigma(l_2) = k_y(v_3(l_2) - v_2(l_2)), \tag{15}$$

$$\tau(l_2) = k_z\left(w_3(l_2) - w_2(l_2) + \frac{1}{2}H_2 v_3'(l_2) + \frac{1}{2}H_1 v_2'(l_2)\right). \tag{16}$$

The available energy release rate is

$$\mathcal{G} = \mathcal{G}_I + \mathcal{G}_{II} \tag{17}$$

where

$$\mathcal{G}_I = \frac{1}{2}\frac{\sigma(l_2)^2}{k_y} \tag{18}$$

$$\mathcal{G}_{II} = \frac{1}{2}\frac{\tau(l_2)^2}{k_z} \tag{19}$$

are the contributions related to fracture modes I and II, respectively.

Furthermore, we compute the mode-mixity angle as follows:

$$\psi = arctan\sqrt{\frac{\mathcal{G}_{II}}{\mathcal{G}_I}}. \tag{20}$$

According to the chosen mixed-mode fracture criterion, the critical value of $\mathcal{G}$ is estimated by the formula

$$\mathcal{G}c = \frac{1}{\frac{cos^2(\psi)}{GIc}+\frac{sin^2(\psi)}{GIIc}}, \tag{21}$$

with $\mathcal{G}_{IC}$ and $\mathcal{G}_{IIC}$ are the values of fracture toughness in modes I and II, respectively.

Figure 8 shows a plot of the available (green curve) and critical (red curve) energy release rates as functions of the compressive axial force in sub-laminate (4). The intersection point between the two curves corresponds to the predicted onset of delamination growth. In this numerical example, delamination growth is expected at P_4 = 378.84 N, corresponding to an applied bending moment M = 1917.1 Nmm/mm. This value slightly underestimates the experimentally measured average bending moment at propagation M = 2725 Nmm/mm [5].

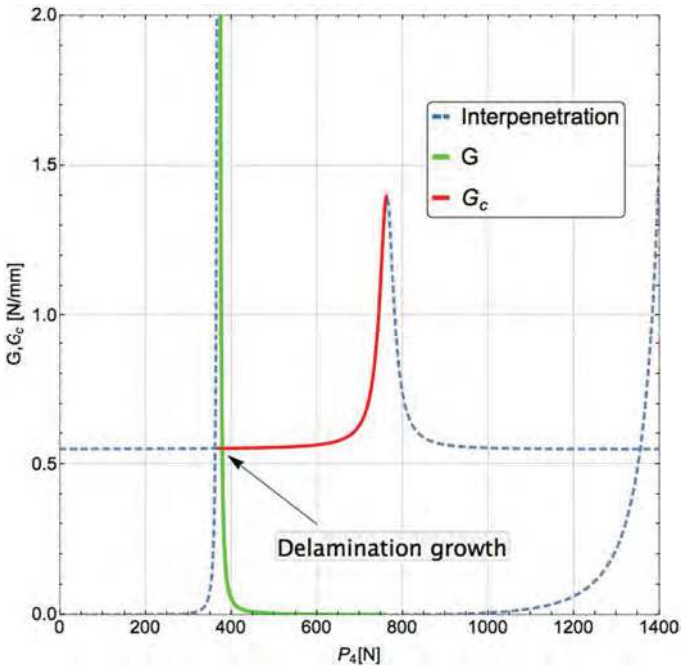

Figure 8: Available and critical mixed-mode energy release rates.

5 CONCLUSIONS

- A mechanical model of a four-point bending test on a delaminated specimen has been developed, whereby the specimen is considered as an assemblage of laminated beams partly connected by an elastic interface.
- The model is described by a differential problem with suitable boundary conditions. An analytical solution to this problem has been determined for both the pre- and post-critical stages.
- The developed model does not take into account explicitly contact between the debonded sub-laminates and interpenetration is not prevented. However, the predicted response

stemming from the model has been filtered out in order to exclude all physically unfeasible responses.

- As a result, the theoretical specimen response has been figured out and compared with some experimental results taken from the literature.
- A mixed-mode fracture criterion has been applied to predict the onset of delamination.
- The theoretical model proves able to predict the qualitative behaviour observed in the tests, albeit some quantitative discrepancies exist, in particular for the applied bending moment corresponding to the onset of delamination growth.
- Future developments include the design and conduction of *ad hoc* experimental tests to remove any doubts about some uncertain experimental parameters from the literature.
- Besides, the model could be improved in order to explicitly take into account contact, at the price of losing the possibility of a complete analytical solution in favor of some numerical methods.

REFERENCES

[1] V.V. Bolotin, Delaminations in composite structures: Its origin, buckling, growth and stability. *Composites Part B*, **27**, 129–145, 1996.

[2] W. Gong, J. Chen, E.A. Patterson, An experimental study of the behaviour of delaminations in composite panels subjected to bending. *Composite Structures*, **123**, 9–18, 2015.

[3] S. Bennati, P.S. Valvo, An elastic interface model for delamination buckling in laminated plates. *Key Engineering Materials*, **221–222**, 293–306, 2002.

[4] S. Bennati, P.S. Valvo, Delamination growth in composite plates under compressive fatigue loads. *Composites Science and Technology*, **66**(2), 248–254, 2006.

[5] M. Kinawy, R. Butler, G.W. Hunt, Buckling and Propagation of a Delaminated Composite Beam in Bending. *AIAA* SDM *Student Symposium,* 2771, 2010.

[6] M. Kinawy, R. Butler, G.W. Hunt, Buckling and postbuckling of a delaminated composite beam in bending. *AIAA J.* **49**, 670–672, 2011.

[7] M. Kinawy, R. Butler, G.W. Hunt, Bending strength of delaminated aerospace composites. *Philosophical Transactions of the Royal Society A*, **370**, 1780–1797, 2012.

[8] N. Dardano, *Un modello meccanico per la delaminazione promossa da instabilità*. MSc thesis in Civil Engineering, University of Pisa, 2016.

[9] G.A. Kardomateas, Snap buckling of delaminated composites under pure bending. *Composites Science and Technology*, **39**, 63–74, 1990.

[10] Z. Suo, J. W. Hutchinson. Mixed Mode Cracking in Layered Materials. *Advanced in Applied Mechanics,* **29**, 64-187, 1992.

APPENDIX

The constants entering the analytical solution in the post-critical regime have the following expressions:

$$\chi_2 = H_1^2(EH_2^3(\alpha^2+\beta^2)(EH_2(5\alpha^4-10\alpha^2\beta^2+\beta^4)+(2\beta^2-6\alpha^2)k_z)+ \\ -12k_y(k_z-EH_2(\alpha^2+\beta^2)))+2H_2H_1k_z(EH_2^3(-3\alpha^4-2\alpha^2\beta^2+\beta^4)+12k_y)+ \\ +36H_2^2k_yk_z \tag{22}$$

$$\omega_2 = H_1^2\Big(12k_y(EH_2(\alpha^2+\beta^2)+k_z)+EH_2^3(\alpha^2+\beta^2)(EH_2(\alpha^4-10\alpha^2\beta^2+5\beta^4)- \\ 2(\alpha^2-3\beta^2)k_z)\Big)-2H_2H_1k_z\big(EH_2^3(\alpha^4-2\alpha^2\beta^2-3\beta^4)+12k_y\big)+ \\ -36H_2^2k_yk_z \tag{23}$$

$$\zeta_2 = -2H_2H_1k_z\big(E\gamma^4H_2^3+12k_y\big)+H_1^2\Big(12k_y(k_z-E\gamma^2H_2)-E\gamma^4H_2^3(E\gamma^2H_2+2k_z)\Big)+ \\ -36H_2^2k_yk_z \tag{24}$$

$$\chi_3 = H_1^2(EH_2(\alpha^2+\beta^2)-k_z)+2H_2H_1k_z+3H_2^2k_z \tag{25}$$

$$\omega_3 = H_1^2(H_2E(\alpha^2+\beta^2)+k_z)-2H_2H_1k_z-3H_2^2k_z \tag{26}$$

$$\zeta_3 = H_1^2(\gamma^2H_2E-k_z)+2H_2H_1k_z+3H_2^2k_z \tag{27}$$

$$D_1 = \frac{1}{3\gamma(H_1-H_2)H_2^2(H_1+H_2)(\alpha^2+\beta^2)k_z} \tag{28}$$

$$D_2 = 2C_{15}(H_1-H_2)(H_1+H_2) \tag{29}$$

$$D_3 = 3C_{14}(H_1-H_2)H_2k_z-3C_{17}(H_1-H_2)H_2k_z \tag{30}$$

$$D_4 = 6C_{13}(H_1-H_2)H_2k_z-6C_{16}(H_1-H_2)H_2k_z+12EC_{15}H_1(H_1-H_2)H_2 \tag{31}$$

$$D_5 = 3C_{18}(H_1-H_2)H_2(H_1+H_2)k_z+6EC_{14}H_1^3 \tag{32}$$